Complex cementation textures and authigenic mineral assemblages in Recent concretions from the Lincolnshire Wash (east coast, UK) driven by Fe(0) to Fe(II) oxidation

Article *in* Journal of the Geological Society · February 1995

DOI: 10.1144/gsjgs.152.1.0157

CITATIONS
34

READS
57

4 authors, including:

Mohammed R Al-Agha
Islamic University of Gaza
40 PUBLICATIONS **361** CITATIONS

SEE PROFILE

Stuart D Burley
Keele University
118 PUBLICATIONS **1,538** CITATIONS

SEE PROFILE

Journal of the Geological Society, London, Vol. **152,** 1995, pp. 157–171, 10 figs. 1 table. Printed in Northern Ireland

Complex cementation textures and authigenic mineral assemblages in Recent concretions from the Lincolnshire Wash (east coast, UK) driven by Fe(0) to Fe(II) oxidation

M. R. Al-AGHA[1,2], S. D. BURLEY[1], C. D. CURTIS[1] & J. ESSON[1]

[1]*Diagenesis Research Group, Department of Geology, University of Manchester, Manchester M13 9PL, UK*

[2]*Department of Geology, Islamic University of Gaza, PO Box 108, Gaza, Gaza Strip*

Abstract: Concretions are common in some of the modern intertidal sediments on the Lincolnshire coast of the Wash. The mineralogy and geochemistry of numerous examples of these concretions have been studied in detail. The majority have metallic nuclei and those that do not, exhibit textures which suggest that they originally did so. Petrographic observations indicate that the cements within these concretions precipitated in a distinct sequence that is spatially developed around the metallic nucleus and that are arranged from core to periphery: (a) a ferrous hydroxy chloride mineral (similar in bulk composition to akaganeite) together with iron monosulphide (amorphous FeS and mackinawite), pyrite and possibly elemental sulphur; (b) ferroan carbonate cements (including siderite, ankerite and calcite); (c) mixed ferrous and ferric minerals ("green rust" together with magnetite and possibly greigite); (d) fully oxidized minerals (including akaganeite, goethite, hematite, gypsum and a complex basic sulphate of Fe, Ca, Mg, Si and Al). This latter material has not been possible to characterize fully but is probably an amorphous mixture.

The initiating reaction for the precipitation of these cements is anaerobic corrosion of iron at zero valence state with sulphate as an oxidant. Metal, hydroxide and monosulphide are found in close spatial association, indicating the reaction:

$$4Fe^0 + SO_4^{2-} + 4H_2O \rightarrow 3Fe(OH)_2 + 2OH^- + FeS$$

Further away from the metallic nucleus, carbonates cement the host clastic sediment. These are the products of reaction between the first-formed hydroxides and pore water solutes (principally HCO_3^-, Mg^{2+} and Ca^{2+}). When oxygen gains access to the growing concretion, Fe(II) minerals are replaced very rapidly by akaganeite and either goethite or hematite. Gypsum and other sulphate minerals also precipitate as new cements around the periphery of the concretions.

The cementation process in these concretions is driven by the extreme instability of metallic iron (here, relic military armaments and shrapnel fragments) in contact with saline, anaerobic water and is indicative more of cathodic corrosion than the growth of ancient carbonate–sulphide concretions.

Keywords: concretions, modern, diagenesis, intertidal environment, Lincolnshire England.

Concretions have stimulated widespread interest for many years. Originally they were sought for the exquisite fossils not uncommonly preserved within them. More recently, sedimentologists and geochemists have obtained numerous chemical and isotope data from the various cement minerals present within concretions in order to learn more about the post-depositional history of ancient sedimentary rocks (e.g. Gautier 1982; Scotchman 1991). A limitation of this approach, however, results from the common difficulty of relating ancient concretion growth to the geochemical environment of mineral authigenesis. The use of modern analogues to overcome this problem, where concretions seen to be forming now can be studied *in situ* directly within their ambient environment of formation, has been impeded by the relative rarity of such concretions. This is especially the case for marine muds.

Concretions are forming today in intertidal marsh sediments of the Wash near Warham, Norfolk, on the east coast of the UK, and have been suggested to represent analogues of ancient siderite concretions (Pye 1982; Pye *et al.* 1990). These concretions are iron-rich and reported to be variously cemented by hydrated iron oxides, iron sulphides, siderite, ankerite, calcite and gypsum. Siderite cements are more frequently described from fresh and brackish water environments (Ho & Coleman 1969; Postma 1977, 1982; Stoops 1983; Moore *et al.* 1992) whereas pyrite, magnesian calcite and aragonite are the early diagenetic minerals most frequently encountered in temperate shallow marine sediments (Van Straaten, 1957; Coleman & Gagliano, 1965; Wiedemann 1972; Jorgensen 1976; Al-Hashimi 1977; Adams & Schofield 1983). In terms of their mineralogy, therefore, these Recent concretions from the coast of eastern England exhibit a remarkable diversity and appear to be the result of formation from mixed, rather complex geochemical environments.

Pye *et al.* (1990) also point out that the Warham concretions are remarkable for the rapidity of their formation. Model calculations (e.g. Berner 1968; Wilkinson & Dampier 1990) suggest that whilst on a geological time scale carbonate concretions form rapidly, they typically take several thousands of years to develop. Along the north Norfolk coast, however, concretions up to 0.4 m in diameter can be shown to have grown in marsh sediments accreted since the Second World War.

The work described here was undertaken on Recent concretions collected from intertidal marsh sediments of the Lincolnshire Wash, similar to those described by Pye *et al.* (1990) from the north Norfolk coast. A comprehensive

description of the petrography, mineralogy and chemistry of the various authigenic cements within these present-day concretions is used to provide a better basis for discussion of the concretion growth processes than has hitherto been possible. These data are then used to consider the relevance of the Recent concretions from the Wash as possible analogues for ancient concretions.

Study area and its modern sedimentology

The Wash is a large macrotidal embayment situated on the eastern seaboard of England, off the Lincolnshire and Norfolk coasts (Fig. 1). The embayment is fringed by a variable belt of fenlands, saltmarshes and intertidal sediments, that are arranged roughly parallel to the coastline. Low tide exposes a broad intertidal zone of readily accessible active mud and sand sedimentation that is typically 2 km wide and locally exceeds 10 km width.

The intertidal zone of the Wash in south Lincolnshire, from Freiston in the south towards Gibralter Point in the north, comprises a series of well defined sedimentological zones, starting on the landward edge with vegetated saltmarsh and passing through mudflats and sandflats seawards (Fig. 1). In detail, these zones were subdivided further by Evans (1965) into saltmarsh, higher mudflat, inner *Arenicola* sandflat, lower mudflat and lower sandflat. Evans (1965, 1975) described the sedimentology and biology of these zones in detail, and estimated the thickness of the tidal flat sequence to be in excess of 7 m, although the base of the tidal sand sequence at Freiston was not recorded. Processes of deposition on the intertidal zone were documented by Evans & Collins (1975) and Collins *et al.* (1981) who showed that each tidal flood brings vast quantities of suspended and bed load sediment over the intertidal zone. Much of this sediment is deposited in response to the decrease in energy of the advancing tidal wave and results in the grain size differentiation of sediments across the intertidal zone. Suttill *et al.* (1982) calculated an overall sedimentation rate for the tidal flat of 1.5 mm per year over the last 1000 years which is directly comparable to estimates of the combined rate of rise of sea level and subsidence in the Wash over the same time period (Coles & Funnell 1981).

For the purpose of this study we briefly describe the salient features of the main depositional zones in transects across the intertidal zone at Freiston and Leverton (lines A–A′ and B–B′ respectively in Fig. 1). We simplify the sedimentary facies designations described by Evans (1965) and recognize saltmarsh, higher mudflats, sandflats and an

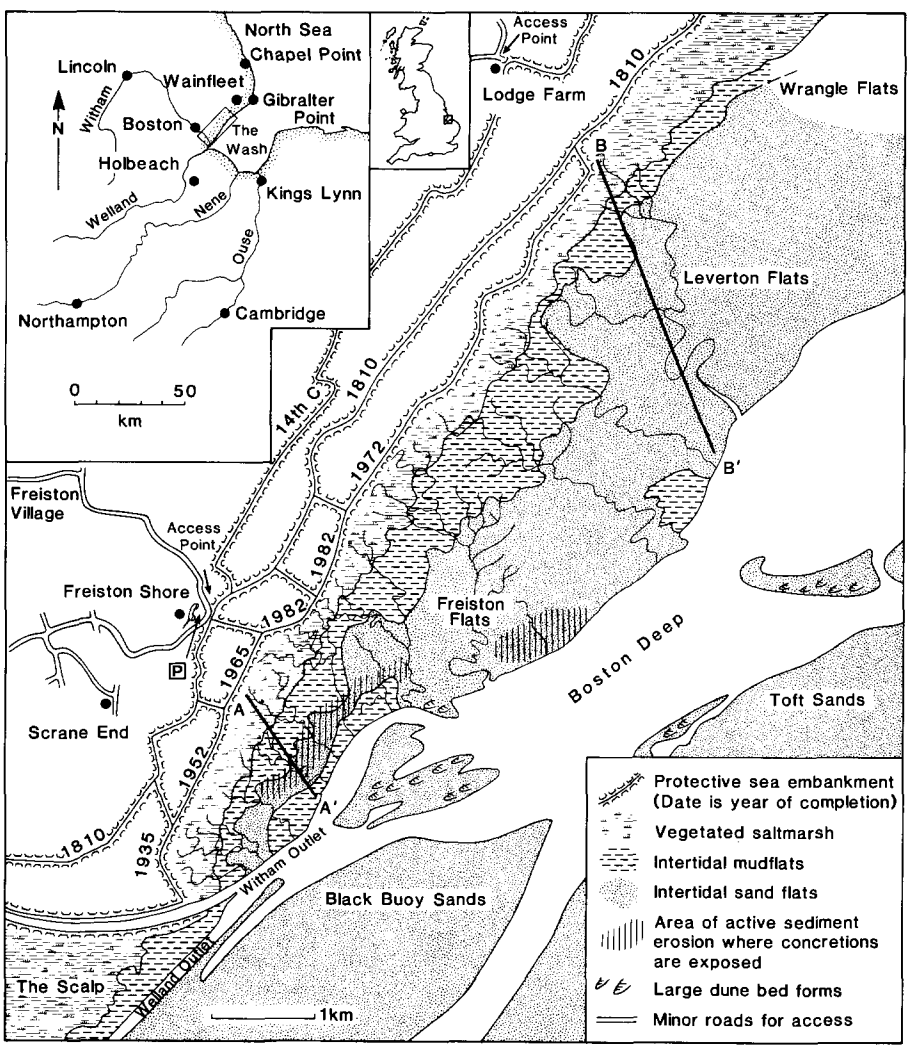

Fig. 1. Sketch map of the coastal belt between Freiston and Leverton showing the distribution of the main intertidal sediment facies and the historical development of the sea defence embankments. Sample collection was made along lines A–A′ and B–B′. Access points at Freiston Shore and Lodge Farm, Leverton are shown. Insets indicate the setting of the field area in relation to the Wash embayment and the UK.

irregular belt of sporadically developed muds close to the low tide mark that are broadly equivalent to the lower mudflats of Evans (1965).

The saltmarsh sediments consist of silty sands and clayey silts which are intensely vegetated and well stabilized as a result of algal mat and higher plant colonization. Lamination is weakly preserved but root channels penetrate throughout the sediments. Interbedded coarse sand layers are present, being most readily seen close to creeks and probably represent either levee deposits or the channel lag deposits of older tidal creeks. The degree of plant colonization varies seasonally (Fig. 2a & b) but decreases progressively seawards across the saltmarsh.

The higher mudflats are dissected by numerous tidal creeks (Fig. 2a). These actively meander across the mudflats during the ebb flow and rework the tidal deposits. The edges of creeks that erode down through these mudflats, and the walls of trenches dug in them, display low-angled cross-stratification as a result of tidal channel migration comparable to that described by de Mowbray (1983) for equivalent mudflats of the Solway Firth. The mudflats are covered with a film of algal mat and are extensively burrowed, although not as pervasively as the sand flats.

Shallow inter-creek depressions, referred to as pans, are common on both the lower edge of the saltmarsh and across the higher mudflats (Fig. 2a & b). Pans are crudely oriented SW–NE, parallel to the dominant wind direction across the intertidal flats. In winter months they are usually filled with sea water (Fig. 2a). They probably originated as oxbows of abandoned tidal creek meanders, but their present shape and orientation results from the wind driven, pan water erosion of the mudflats. During the summer, the mudflats and pans dry out between high tides, and are covered with desiccation cracks (Fig. 2b). The cracks and burrows are typically bound by algal coatings and cemented by brown coloured iron hydroxides such that they now stand above the surface of the mudflats.

The lower edge of the higher mudflats has undergone considerable erosion. Much of this is known from aerial photographs and local knowledge to have taken place since

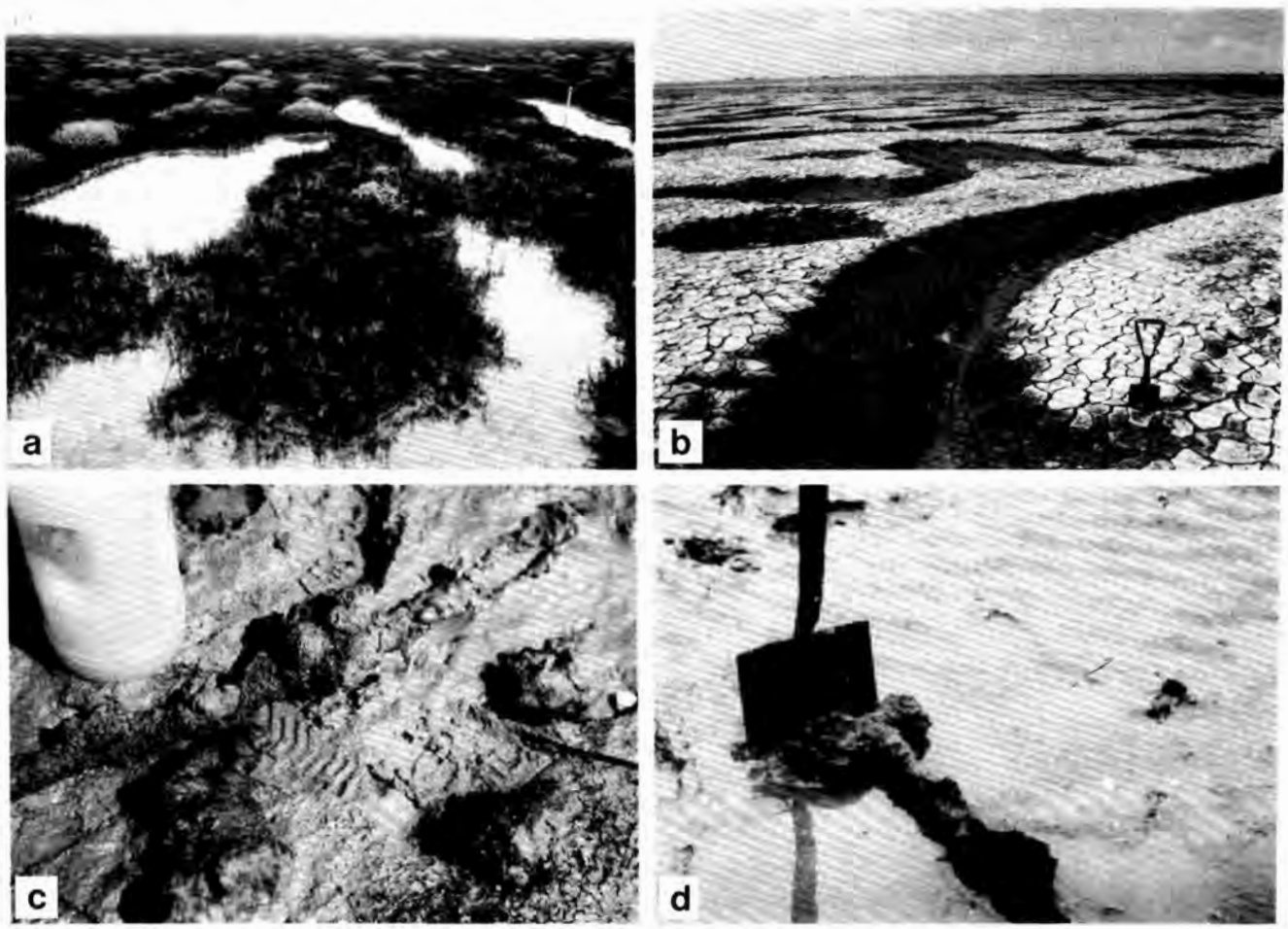

Fig. 2. The Wash intertidal zone and field appearance of the concretions. **(a)** View across the intertidal zone taken at the beginning of winter looking towards the 1982 embankment at Freiston Shore. Note the vegetation and the water-filled pans between the tidal creeks. **(b)** Similar view taken during high summer showing the typical development of desiccated upper mudflats illustrating the seasonal variation in the character of the upper marsh. **(c)** A collection of concretions from immediately below the sandflat surface. The small sperical concretions all contained metal fragments whilst the elongate concretions contained relic metal rods. Drink container is 30 cm high. **(d)** A large concretion developed around an iron tube dug out of the sandflats at Freiston. The concretion was found a few centimetres below the rippled sand surface. The black interior of the concretion is visible. Width of spade is 20 cm.

the building of the latest sea embankment in 1982, although earlier erosion of the mudflats is documented by Collins *et al.* (1981). Erosion has exposed the underlying tidal sands which have been extensively modified by tidal currents into sandwaves and dunes, and ebb currents have variously reworked these sandflats resulting in a complex surface. The sandflats have also accreted landwards as a result of new sand addition introduced during each tidal cycle (Collins *et al.* 1981). The largest area of sand flats is developed on the Leverton Flats (Fig. 1). Here the tidal creeks are much larger and more stabilized than on the sand flats at Freiston although they are still observed to actively meander during the ebb flow.

At Freiston a lower area of very recent mud deposition, probably equivalent to the lower mudflats of Evans (1965), is present close to the low water mark. These muds are very soft and unconsolidated and have been deposited in the last few years, possibly in response to construction of the latest sea embankment.

The vertical sedimentary sequence, diagenetic zonation and location of the concretions

A schematic cross section through the intertidal zone shows the idealized vertical distribution of sediments (Fig. 3). Beneath the laminated marsh muds and mudflat sediments is a laterally persistant tidal marine sand that has been proved to a depth of 12 m at Freiston (Suttill *et al.* 1982; A. Boult pers. comm. 1992), but which is known from the coastal section at Chapel Point, some 15 km north of Gibralter Point (see Fig. 1 inset map), to be underlain by a pre-Roman period of brackish water marsh sequence, Iron Age peat deposits and glacial clay (Swinnerton & Kent 1976).

On the upper marsh, the majority of the sediments are oxygenated to a depth of about 2 m and are light brown or grey in colour. Below this depth, the sediments are permanently waterlogged and are black and anoxic. Adjacent to major creeks and in the marsh sediments beneath the pans the zone of oxygenation is greatly reduced in thickness and typically penetrates only a few millimetres beneath the surface.

On the intertidal sand flats, the zone of oxygenation reaches a maximum of about 50 cm but the thickness of this oxidized layer thins dramatically towards the low tide mark. The actual thickness of the oxygenated layer depends significantly on the host sediment lithology, and this effect is seen clearly on the lower intertidal flats. Here, in the sands 2–3 cm of the upper sediment may remain oxygenated whilst in the muds it is restricted to the top 2–3 mm.

Love (1967) first documented the vertical change in diagenetic mineralogy through these sediments and laterally across the intertidal zone. The upper oxidized zone is present everywhere, although its thickness varies across the flats. The mineralogy of this oxidized zone is dominated by acid soluble ferric hydroxides, which Love (1967) considered as being introduced as detrital material adsorbed on, for example, clay minerals. The thickness of the hydroxide zone is related to the tidally-controlled water table, certainly in the sand lithologies, although the higher mudflat and saltmarsh sediments appear to be essentially impermeable and the water table is suppressed in these sediments. Beneath this zone the sediments are black and anoxic, and contain iron monosulphide minerals (Fig. 3). Oxygen brought into this zone along mudcracks and through the activities of benthic organisms oxidizes the immediately adjacent muds.

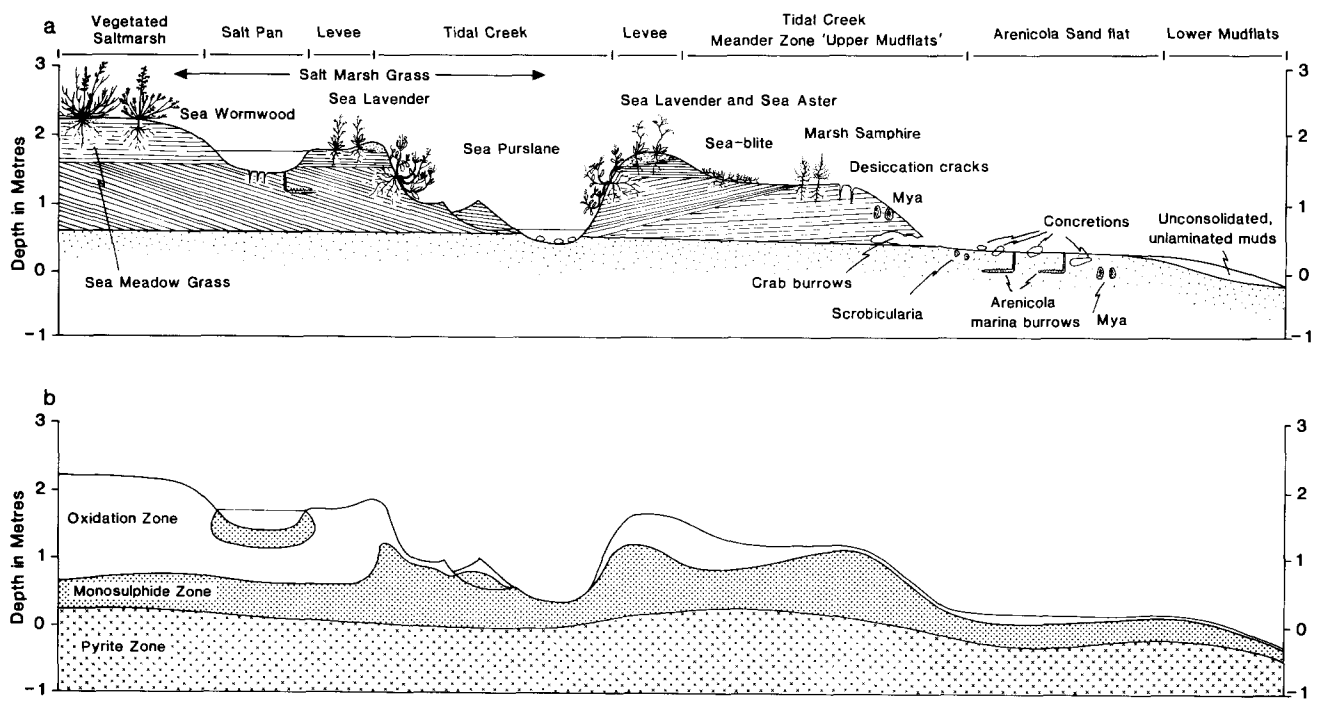

Fig. 3. Schematic cross-section through the intertidal zone at Freiston (along transect A–A′ in Fig. 1) illustrating the vertical and lateral extent of the sedimentary features and the distribution of diagenetic zones, based partly on Love (1967). Vertical scale greatly exaggerated and size of tidal creeks not in proportion to width of intertidal zone.

Approximately 50–70 cm below the monosulphide layer, and usually coinciding with the occurrence of the tidal sands, the sediments turn grey coloured and Love (1967) records the presence of pyrite framboids in them. Love (1967) argues that the transformation of monosulphide to pyrite takes place *in situ*, and that the pyrite inherits both the morphology and size distribution of its monosulphide precursor.

Concretions are exclusively seen in the tidal sands of the pyrite zone, and appear in all cases to be concentrated in the upper part of these sediments. No concretions have been recovered from the equivalent anoxic zone on the flanks of tidal creeks or beneath pans, although reworked, partially oxidized concretions are found as lag concentrates in some of the tidal creeks. Most of the concretions from the Lincolnshire Wash have been recovered from the sand flat surfaces, especially in the upper sand flats at Freiston where erosion is currently removing the lower mudflat sequence (along transect A–A′ of Fig. 1). After winter or spring storms fresh concretions are commonly exposed on the sand flat surface, and digging in the vicinity of exposed concretions usually reveals many more in the top few centimetres of the sand flat sediments (Fig. 2c & d). The majority of the concretions are *c.* 10–20 cm in diameter, but their shape and size varies greatly and in most cases is governed by the shape of the nucleus they have grown around. It is obvious that many have grown around iron or steel nuclei and they can exceed 1 metre in diameter (determined by the size and shape of the original metallic nucleus; see Fig. 2c & d). Pebbles and calcareous shell fragments are frequently incorporated in the concretions by cementation. The concretions are black when fresh, but brown or orange oxidation rims develop very rapidly on exposure to air.

Land reclamation and anthropogenic activities

In the Holocene, the Fenland of eastern England was a low-lying swamp which was gradually inundated by the post-glaciation rise in sea level (Coles & Funnell 1981; Shennan 1982, 1987) and became the inner part of a wide coastal lagoon and brackish water marshland complex protected by an outer sand barrier. As the sea continued to rise, the barrier bar complex migrated landwards and prograded across the deposits of the brackish swamp, depositing the so-called fen 'silt-lands' in a wide crescent around the margins of the Wash. The modern tidal flat environment in the Wash is the result of the Romano-British marine transgression of 300BC (Godwin & Clifford 1938; Shennan 1986*a*, *b*).

Since Saxon times, man has interfered with the natural sedimentary processes of the fen wetlands bordering the present day Wash to the extent that the present shape of the Wash is a result of successive periods of reclamation. Around most of the perimeter of the Wash an artificial embankment serves to prevent marine flooding of the reclaimed marshland.

Systematic reclamation of the Wash fenlands began with the construction of the 'Roman Bank' in the thirteenth and fourteenth centuries and continues to the present. Some 1500 km^2 of land has been reclaimed since the seventeenth century when reclamation began in ernest in an attempt to drain the fenlands through a programme of land drainage and river engineering. In recent times a series of sea embankments were constructed from 1935 with the latest embankment at Freiston being completed in 1982 (Fig. 1).

The construction of embankments and reclamation result in an increase of sedimentation on the upper marshes and a gradual seaward advance of the saltmarsh and the adjacent mudflats, but it appears that the low water mark does not advance progressively seawards (Doody 1987). As a result there is a progressive narrowing of the intertidal zone with successive land reclamations and, in some areas of the intertidal zone, the upper mudflats merge with the lower mudflats and the intervening sand flats are covered in mud. This can be seen around the Witham outfall and may be responsible for the mud accretion on the Freiston flats and the associated erosion of the sand flats and the higher mudflats.

The intertidal zone has been used as a bombing range and site for military exercises (in common with the intertidal flats around much of the Wash) since the establishment of an artillery range from Freiston Shore to Wainfleet in 1891 by the First Lincolnshire Artillery Regiment (Curtis 1987). Intermittent use of the range continued through the First World War, when Freiston and Wrangle flats were used for aerial bombing trials. The area was defended as a potential invasion site during the Second World War, and has remained in the flight path of RAF bombing training exercises at Wainfleet ever since. The intertidal flats are now littered with the debris of these activities, including munitions and the remains of several aircraft crashes.

Investigation methods

Some 80 concretions were collected over a period of three years and several sampling excursions to the Wash. Of these concretions, 35 have been investigated in detail. In the field, after removal from the intertidal sediments, the concretions were immediately placed in plastic containers which were filled with sea water to minimize aerial oxidation and the containers were then sealed.

Once in the laboratory, the concretions were stored under water in sealed jars. All the concretions were subsequently cut with a diamond saw and the cut surface polished and examined. A representative selection of the cut concretions were photographed and impregnated with epoxy. Polished thin sections were prepared in paraffin from 35 of the concretions and then carbon coated and stored in a vacuum desiccator to minimize oxidation effects.

The petrography and textures of the concretions were studied in thin section employing both transmitted and reflected light optical microscopy as well as in the SEM using back-scattered electron (BSE) imagery. Freshly cut or fractured material was sub-sampled with a microdrill for XRD analysis of specific areas of the concretions to determine their mineralogy. Particular care was taken to sample and analyse the different textural zones which develop around the metallic nuclei and that are clearly discernable in hand specimen. The chemical composition of the authigenic cements was determined quantitatively with EDS analysis using a Jeol 6400 SEM and with WDS/EDS using a CAMECA electron microprobe.

Mineralogy and composition of concretion cements

Most of the concretions collected proved to contain a metallic nucleus (Fig. 4a). These are presumed to be the remains of fragments of military shells and other hardware from either wartime or subsequent training exercises. Those concretions that do not now contain a metal nucleus exhibit textures suggestive of the former presence of one.

The mineralogy of the sample suite as a whole was established from many chemical analyses (using both

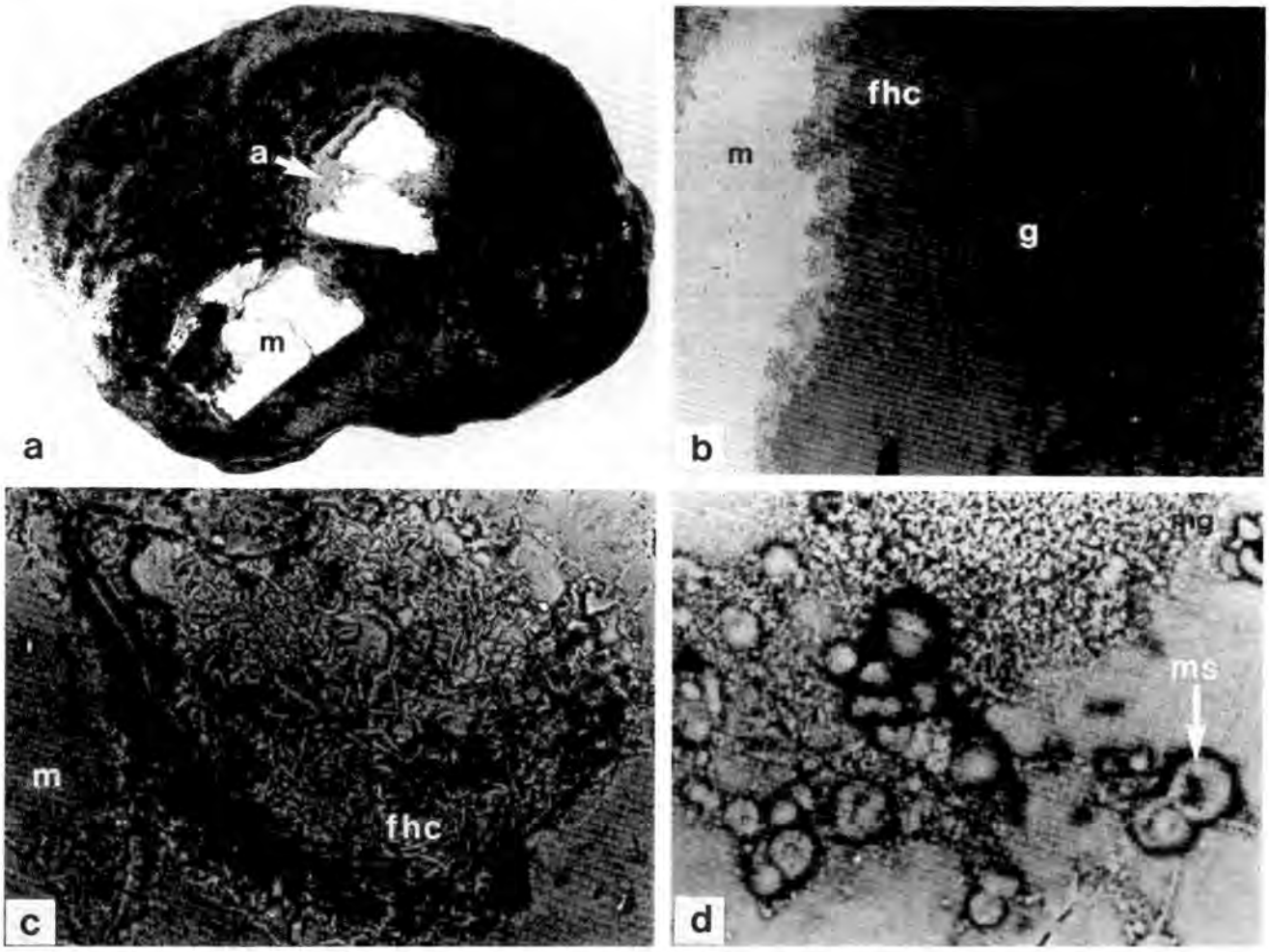

Fig. 4. Aspects of the concretions and their mineralogy. (**a**) Polished section cut through a typical concretion showing the presence of metal iron nuclei (m). Note replacive alteration zone (arrowed a) around the nucleus and the crudely concentric structure to the concretion. Width of concretion = 6.75 cm. (**b**) BSE-SEM micrograph showing the contact between the metal nucleus (m) and ferrous hydroxide chloride (fhc, now akaganeite where oxidized) and goethite (g) corrosion products together with the adjacent, enclosing host cemented detrital sediment. Width of micrograph = 6 mm. (**c**) Details of the crystal growth texture commonly developed in ferrous hydroxide chloride (fhc) in cavities on the surface of the metal nucleus (m). BSE-SEM micrograph. Width of micrograph = 250 μm. (**d**) FHC microsphere (example arrowed, ms) and microgranular (mg) replacement textures developed in the metal nucleus. BSE-SEM micrograph. Width of micrograph = 20 μm.

microprobe and SEM-EDS) coupled with XRD crystal structural data. A full characterization of the authigenic mineralogy of the concretions actually proved to be very difficult to achieve because few of the minerals gave good X-ray reflections and some are apparently amorphous. Repeat XRD traces were taken to establish whether unknown minerals were oxidation product artifacts, as some of the primary authigenic minerals are unstable in air and rapidly decompose whereas oxidation product XRD reflections strengthen with time.

Minerals (or their amorphous analogues) identified include a ferrous hydroxide-chloride, an acid volatile monosulphide (probably mackinawite), pyrite, elemental sulphur, ankerite, siderite, Fe-calcite, Mg-calcite, 'green rust', magnetite, possibly greigite, akaganeite, goethite, hematite, gypsum and a complex, amorphous sulphate mineral which has not been possible to characterize fully. Chemical composition data expressed as averages for some of these minerals are given in Table 1.

Petrography and formation mechanisms of individual cements

Ferrous hydroxide-chloride (FHC)

Examination of metallic cores in optical thin section showed them to be surrounded by a dark green, transparent lath-shaped mineral together with lesser amounts of an opaque, amorphous-appearing sulphide. In concretions exposed to air these minerals are surrounded by and intimately mixed with goethite (Fig. 4b). The amount of goethite increases with the degree of oxidation. SEM micrographs reveal that microcracks in the metal nucleus are invariably filled with a fibrous mineral that has precipitated from the microfracture walls and exhibits a growth habit comparable with that of the transparent green coloured mineral. Other textural details associated with the metallic cores are illustrated in Fig. 4c & d. Aggregates of microgranular, lath and filament shaped crystals coat the

Table 1. *Chemical composition (wt%) of authigenic minerals in the Wash concretions*

	FHC 17	SD	Akagan. 14	SD	Goeth. 11	SD	Mackin. 7	SD	Pyrite 11	SD	Siderite 13	SD	Calcite 22	SD	Ankerite 9	SD
SiO_2	0.40	0.10	0.38	0.12	0.40	0.11	b.d.	b.d.	0.34	0.01	0.36	0.12	0.31	0.11	0.41	0.17
TiO_2	0.04	0.04	0.35	0.04	0.02	0.04	b.d.	b.d.	b.d.	b.d.	0.02	0.03	0.05	0.06	0.02	0.03
Al_2O_3	0.05	0.06	0.06	0.07	0.04	0.04	b.d.	b.d.	0.03	0.06	0.04	0.04	0.04	0.04	0.05	0.08
FeO	70.93	0.86	69.69	3.19	80.38	6.29	65.76*	0.05	47.45*	0.28	54.88	2.27	0.23	0.36	17.13	8.27
MnO	0.11	0.11	0.35	0.28	0.99	0.82	b.d.	b.d.	b.d.	b.d.	0.55	0.07	0.29	0.15	0.50	0.18
MgO	0.14	0.09	0.13	0.16	0.16	0.09	b.d.	b.d.	0.03	0.06	0.34	0.37	2.45	1.11	4.69	1.13
CaO	0.22	0.18	0.06	0.08	0.05	0.06	b.d.	b.d.	0.08	0.06	1.75	1.60	52.97	1.36	31.40	5.66
Na_2O	0.22	0.16	0.31	0.31	0.39	0.18	b.d.	b.d.	0.29	0.03	0.25	0.15	0.19	0.22	0.48	0.27
K_2O	0.03	0.03	0.06	0.06	0.02	0.02	b.d.	b.d.	b.d.	b.d.	0.02	0.03	0.03	0.04	0.03	0.02
SO_4	0.10	0.10	0.12	0.10	0.10	0.10	34.22*	0.61	52.42*	0.39	0.35	0.24	0.44	0.31	1.25	2.29
P_2O_5	0.04	0.01	b.d.	b.d.	0.03	0.05	b.d.	b.d.	b.d.	b.d.	0.24	0.13	0.23	0.20	0.23	0.15
Cl	6.68	8.55	6.06	1.19	0.69	0.37	b.d.	b.d.	b.d.	b.d.	0.17	0.21	0.06	0.05	0.20	0.07
Total	78.92		77.19		83.26		99.98		99.87		58.95		57.24		56.48	

All the analyses determined by electron microprobe except sulphides (by EDS analysis).
b.d., below detection.
FHC, ferrous hydroxide chloride.
SD, standard deviation.
* These values reported as elemental Fe and S.
The number below the mineral name is the number of analyses.

surface of the metal and occupy cavities within it. Small spherical bodies (typically $<5\,\mu m$ in diameter) are also common, and are usually associated with microcracks and fractures. Microspheres such as these have previously been interpreted as being of microbial origin but we have no direct evidence of this in these samples.

Chemical analyses of these microgranular aggregates, laths, filaments and microspheres (Table 1) suggest they all have a similar composition which is close to that of akaganeite (a crystalline Fe(III) oxy-hydroxide with significant substitution of Cl^- for OH^-) but XRD reflections of microdrill separates of material from adjacent to the metallic nucleus do not correspond to this mineral at all. A positive identification of this material could not be obtained from American Society for Testing Materials (ASTM) reference data, but a few reflections are somewhat similar to those of various Fe(II) hydroxides and chlorides and elemental sulphur. In an attempt to characterize this material better, XRD traces were obtained from smear preparations of fresh samples and repeated after exposure to air for periods of up to 20 days. Initially black, the samples changed to brown in air over a short period of time. Fig. 5 documents structural changes that took place.

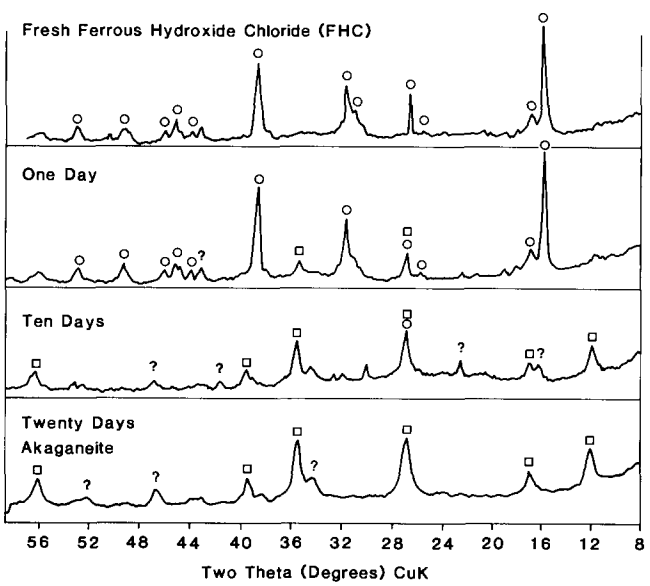

Fig. 5. X-ray diffractograms of corrosion product separated from a concretion core by microdrilling showing the progressive oxidation of ferrous hydroxide chloride (peaks annotated ○) to akaganeite (peaks annotated □) via some undetermined, intermediate crystalline material (peaks annotated ?) over a period of 20 days in air at room temperature.

An unstable, crystalline mineral component with a chemical composition very similar to that of akaganeite is replaced over a period of some 20 days by akaganeite. A second unknown mineral component is formed during exposure to air and decays within the same period and is possibly a reaction intermediate. These observations suggest that the unstable transparent mineral seen intimately associated with metallic iron is probably a Cl^--substituted Fe(II) hydroxide analogous to akaganeite and to which it readily converts on oxidation:

FHC: $Fe_{0.99}(OH)_{1.82}Cl_{0.18}$ (compare with $Fe(OH)_2$)

The zonal sequence typically seen in freshly cut concretions (Fig. 4a & b) is strongly suggestive of a corrosion alteration process that results in replacement of the metallic nuclei from the periphery inwards. Within the anoxic sediments of the Wash the reaction process must be anaerobic:

$$Fe^0 \rightarrow Fe^{2+} + 2e^- \quad \text{anodic reaction} \qquad (1)$$

$$2H^+ \rightarrow H_2 - 2e^- \quad \text{cathodic reaction} \qquad (2)$$

Overall, these electrochemical reactions give:

$$Fe^0 + 2H_2O \rightarrow Fe(OH)_2 + H_2 \qquad (3)$$

Hydrogen would be oxidized rapidly on diffusion away from the vicinity of the metal nucleus (FHC represented by $Fe(OH)_2$, chloride not shown). This is exactly the reaction that is commonly reported for the alteration of archaeological iron artifacts recovered from marine environments (Robinson 1982).

Bearing in mind the ubiquitous presence of iron sulphides in these concretions (see below), anaerobic sulphate corrosion is a likely alternative (or additional) corrosion mechanism:

$$4Fe^0 \rightarrow 4Fe^{2+} + 8e^- \quad (4)$$

$$SO_4^{2-} + 4H_2O + 8e^- \rightarrow 8OH^- + S^{2-} \quad (5)$$

Overall, these reactions can be written:

$$4Fe^0 + SO_4^{2-} + 4H_2O = 3Fe(OH)_2 + 2OH^- + FeS \quad (6)$$

By analogy with $Fe(OH)_2$, the Fe(II) hydroxide-chloride (FHC) would be expected to be extremely reactive with oxygen and also with anionic solutes (see below).

Mackinawite (FeS)

Monosulphides could not be conclusively identified optically in thin section. However, SEM-BSE examination shows that iron sulphides are preferentially located close to the metal nuclei in the concretions and only occasionally cement detrital material in the adjacent sediment. Gel-like textures observed in the SEM in BSE with a high back-scatter coefficient are considered to be monosulphides and are sometimes spatially associated with pyrite framboids. Additionally, very small crystals of a high back scatter coefficient mineral (<1 μm in diameter) occur throughout the concretions (see Fig. 6a & b) and although these crystals proved to be too small to analyse quantitatively, they are iron sulphides and may therefore be mackinawite or its bisulphide stabilized reaction product.

The gel-like material observed in the SEM in BSE closely associated with FHC and metallic Fe gave formulae ranging between $FeS_{0.929}$ and $FeS_{0.948}$ when analysed with EDS (Table 1). These correspond closely with published mackinawite analyses, although diagnostic X-ray reflections as reported by Takeno *et al.* (1970) and Takeno & Clark (1967) could not be obtained from XRD analysis of microdrill separates sub-sampled from adjacent to the metallic cores.

Iron monosulphides are well known to precipitate in anoxic marine muds as a consequence of microbial sulphate and Fe(III) reduction (Love 1967; Berner 1970; Morse *et al.* 1992). The overall reaction can be approximated as follows:

$$2Fe_2O_3 + 4SO_4^{2-} + 9CH_2O \rightarrow 4FeS + 9HCO_3^- + H^+ + 4H_2O \quad (7)$$

Any HS^- produced independently of this reaction would also react with FHC:

$$Fe(OH)_2 + HS^- \rightarrow FeS + H_2O + OH^- \quad (8)$$

Pyrite

Pyrite framboids of up to about 50 μm in diameter are common in the concretions (Fig. 6a & b) and can be observed optically in reflected light and in the SEM in BSE. They comprise around 100 or so individual pyrite crystals, each typically 5 μm in diameter. These framboids are most common close to the concretion cores, but are also disseminated throughout the adjacent host sediment. EDS analyses of framboidal pyrite were close to the theoretical formulae and are consistent with published data (average for 11 analyses $FeS_{1.92}$, compiled in Table 1).

Pyrite is assumed to be the end product of reaction between HS^- and detrital iron minerals in sulphidic sediments although the mechanisms of formation are still incompletely understood (Berner 1984). According to Schoonen & Barnes (1991), the reaction path from amorphous FeS to FeS_2 depends on pH in alkaline

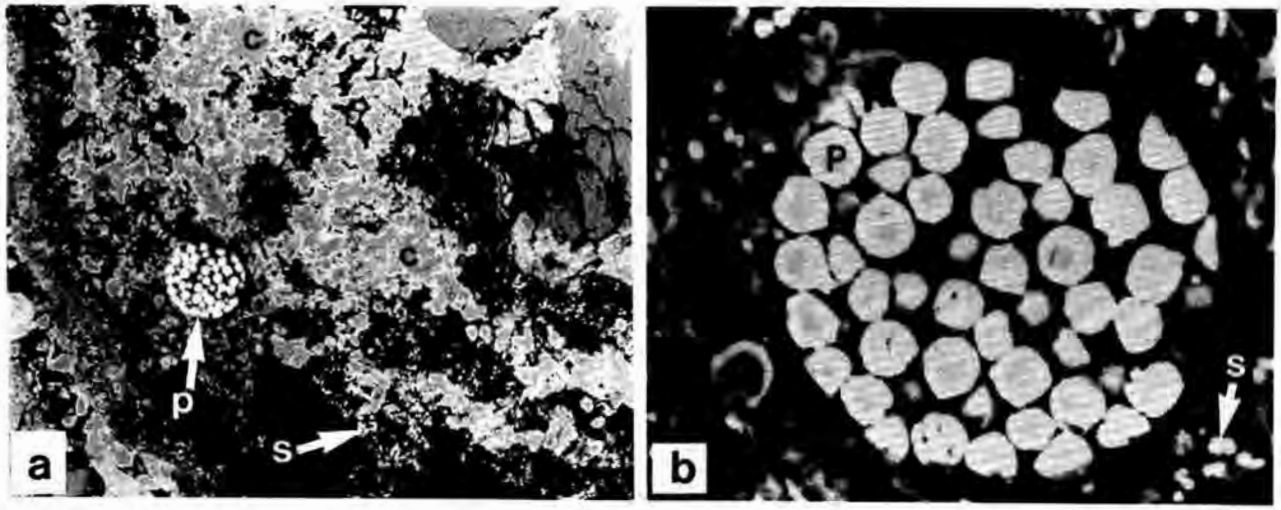

Fig. 6. SEM-BSE photomicrographs of framboidal pyrite cements associated with the metal nucleus. (**a**) Pyrite framboid enclosed in calcite cement (annotated c; overgrown by siderite). Note small dissimented crystals of iron sulphide (arrowed, s). Black areas are porosity. BSE-SEM micrograph. Width of photomicrograph = 300 μm. (**b**) Detail of pyrite framboid (individual pyrite crystal annotated P) and small undefined iron sulphide crystals (arrowed, s). BSE-SEM micrograph. Width of photomicrograph = 50 μm.

solutions. Progressively more sulphur-rich Fe–S minerals are successively formed along the reaction path: amorphous FeS to mackinawite (FeS) to greigite (Fe_3S_4) to pyrite (FeS_2). For greigite to form in this series requires very reducing conditions. Conversion of amorphous FeS to FeS_2 is favoured by relatively more oxidising environments, and pyrite, once nucleated, will grow slowly from solution. Sweeney & Kaplan (1973) demonstrated experimentally that pyrite framboids are formed in the presence of limited oxygen activity (greigite spheres were also produced in these experiments). However, neither greigite nor pyrite formed when oxygen was excluded from their experiments.

Several workers have argued that elemental sulphur is involved in the pyritization process:

$$H_2S + [O] \rightarrow H_2O + S^0 \quad (9)$$

$$FeS + S^0 > FeS_2 \quad (10)$$

In this context it is interesting to recall that the presence of elemental sulphur is suggested in some of the microdrill separates from the textural zone directly adjacent to the concretion cores according to XRD data.

Siderite

Siderite is seen readily in thin section (with both optical and BSEM techniques), and forms a common, often pervasive cement (Fig. 7). The siderite cement is most extensively developed within the host sediments in a zone close to and enclosing the concretion cores and occurs in two distinctive morphologies. The first of these consists of relatively coarse, zoned rhombic crystals that infill the pore space (Fig. 7a & b). More striking is the spheroidal form which is typically pore-lining (Fig. 7c & d). Individual radial crystals in these aggregates tend to be between 20 and 30 μm in length. Textural relationships within any given pore

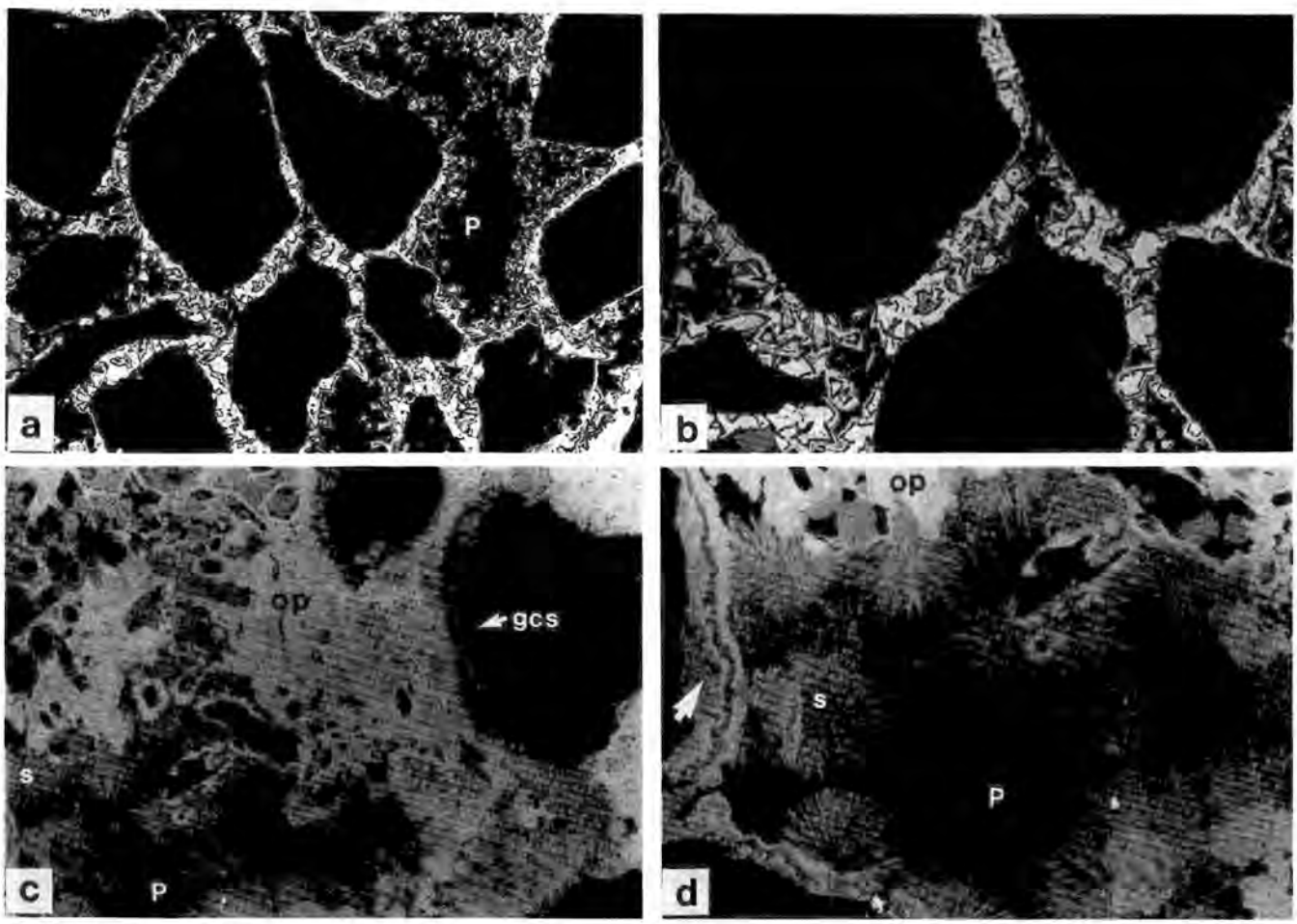

Fig. 7. SEM-BSE photomicrographs of authigenic siderite cements in the concretions. (**a**) General view of showing distribution of zoned rhombic siderite cements that form a pervasive pore filling. Large intergranular pore annotated P. BSE-SEM micrograph. Width of photomicrograph = 450 μm. (**b**) Detail of zoned rhombic siderite cement. BSE-SEM micrograph. Width of photomicrograph = 180 μm. (**c**) Spheroidal siderite coating detrital quartz grains (arrowed gcs) and forming radial aggregates (annotated S) from the host sand flat sediment. The uniform, structureless pore filling material is an undefined oxidation product (annotated op), probably of green rust or monosulphide. Pore space annotated P. BSE-SEM micrograph. Width of photomicrograph = 300 μm. (**d**) Detail of siderite cements. Concentric zoned ankerite-siderite coats detrital grains (example arrowed) and spheroidal siderite (s) nucleates on this coating. Amorphous pore filling material, probably an oxidation product of green rust or monosulphide annotated op. Pore space annotated P. BSE-SEM micrograph. Width of photomicrograph = 180 μm.

indicate that the rhombic siderite cement is an early precipitate which nucleates directly on detrital sand grains, whilst the spheroidal siderite commonly post-dates sulphide cements but pre-dates calcite, akaganeite and gypsum cements (see Figs 7 and 10). Chemical microprobe data for various siderites are given in Table 1 and these analyses include, as expected, minor Ca, Mn and Mg substitution.

Conditions for siderite formation are thought to be quite restricted. Oxygen must be totally excluded, HS^- activity extremely low, HCO_3^- activity high and iron present in abundance (Curtis & Spears 1968). Where corrosion is involved, however, it is not difficult to see how these conditions can be attained. Anaerobic corrosion, either simple (equations 1, 2 & 3) or involving sulphate reduction (equations 4, 5 & 6) generates Fe^{2+} in excess of HS^-. Overall, saturation with respect to Fe^{2+} and OH^- is achieved, any HS^- being stripped out by excess Fe^{2+} (to form FeS). Under these conditions, any HCO_3^- present (either from the marine reservoir, from unstable biogenic carbonates or from microbial oxidation of organic matter) will cause siderite to precipitate:

$$Fe^{2+} + OH^- + HCO_3^- \rightarrow FeCO_3 + H_2O \quad (11)$$

Ankerite

Ankerite is found as a relatively minor pore filling cement within the host sands. Texturally, the ankerite is often seen in thin section to be associated with siderite and calcite cements which it commonly overgrows and is readily distinguished using BSE and EDS analysis in the SEM. The composition of this carbonate was determined by electron microprobe analysis (as listed in Table 1) and corresponds to a typical, Ca-rich formula (mean of nine analyses):

$$Ca_{0.62}Fe_{0.24}Mn_{0.01}Mg_{0.13}CO_3$$

It seems likely that these ankerite cements developed partly from dissolution of unstable (or destabilized) biogenic calcite or aragonite:

$$2CaCO_3 + Fe^{2+} + Mg^{2+} + 2HCO_3^- + 2OH^- \rightarrow 2Ca(MgFe)(CO_3)_2 + 2H_2O \quad (12)$$

Fe,Mg-calcites

Authigenic calcite is most commonly developed away from the centres of concretions where it typically forms a pervasive pore filling cement (Fig. 8). Two distinct

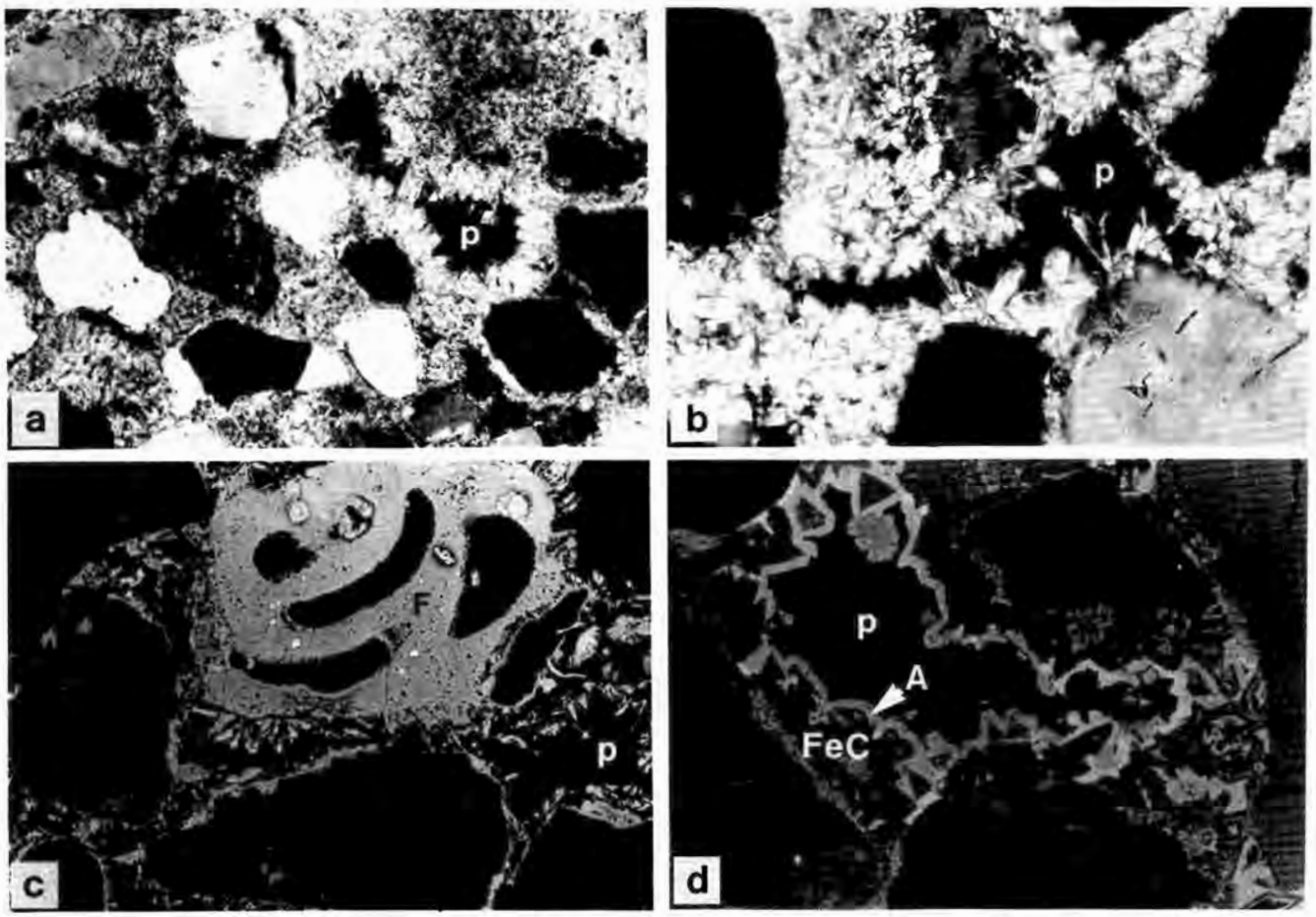

Fig. 8. Optical and BSE-SEM photomicrographs of calcite cements. (**a**) Pervasive pore filling, blocky high-Mg calcite cement. Note the detrital grain rimming, radial calcite growth fabric. Transmitted light photomicrograph, crossed polars. Width of photomicrograph = 400 μm. (**b**) Detail of grain rimming, acicular ferroan calcite cement. Transmitted light photomicrograph, crossed polars. Width of photomicrograph = 220 μm. (**c**) Zoned ferroan calcite cements fringing detrital quartz grains and foraminifera bioclast (annotated F). BSE-SEM micrograph. Width of photomicrograph = 180 μm. (**d**) Zoned ferroan calcite cements (annotated FeC) enclosed in ankerite (arrowed, A), lining pore in host sediment. BSE-SEM micrograph. Width of photomicrograph = 180 μm. Pore space annotated P in all photomicrographs.

morphologies of calcite are present, comprising blocky, tabular crystals (Fig. 8a) and a more acicular, lozenge shaped crystal habit (Fig. 8b) which correspond to magnesian and ferroan compositions respectively (Table 1) . Both magnesian and ferroan varieties are found together in individual examples and may be intimately associated. Calcite cements also occur as coatings to bioclastic shell material (Fig. 8c) but the presence of such grains does appear to enhance the degree of cementation. In BSE-SEM most of the calcite cements are seen to be compositionally zoned, and may be overgrown by either ankerite or siderite cements (Fig. 8d).

As with the ankerite cement, it seems likely that these calcites developed partly from dissolution of unstable (or destabilized) biogenic calcite or aragonite material, but may also be derived from the microbial oxidation of organic matter. Ferroan calcites would be expected to be stable under reducing conditions similar to those favouring both siderite and ankerite precipitation whilst the non-ferroan magnesian calcites should precipitate when iron activity is low, either under oxidising conditions (Fe stripped to form goethite, akaganeite, etc.) or when there is excess HS^- available (Fe stripped as FeS under conditions of intensive sulphate reduction). In the concretions studied here, the former reaction seems more likely.

Green rust (II) (mixed valence oxide–hydroxide)

Fresh concretions containing a metallic nucleus contain in hand specimen a dark greenish black material developed adjacent to the nucleus. On exposure to air this material alters very rapidly (over only a few tens of minutes) to a brown coloured material. As a consequence, it is extremely difficult to characterize this material and effectively impossible to observe it in thin section. XRD analysis of the fresh material shows diffraction peaks characteristic of 'green rust II'. During exposure to air over a four-day period, the strong diffraction peaks from 'green rust II' disappear altogether, with only X-ray amorphous products remaining (Fig. 9). In this respect, 'green rust II' is as unstable as FHC and the iron monosulphides.

In thin section a rather diffuse, amorphous-appearing opaque material is present in many of the samples and may represent the oxidation product of green rust. This material is optically structureless and when viewed in the SEM with BSE is also devoid of resolvable crystalline structure (see Fig. 7c). Various textural relationships with other authigenic cements are developed but it is commonly enclosed in carbonate cements. EDS analysis provides inconsistant iron-rich chemical compositions that are frequently contaminated with silicon and aluminium. However, the combined lack of resolvable structure, its X-ray amorphous nature and variable chemical composition make this material extremely difficult to confirm as an oxidation product of green rust.

Bernal *et al.* (1959) and McGill (1967) describe green rusts, confirm their mixed Fe(II)–Fe(III) valence state and note that these compounds, together with magnetite, are common corrosion products of metallic iron in water. More detailed studies of green rust formation, alteration and environmental controls have been reported by Schwertmann & Taylor (1977), Taylor & Schwertmann (1974) and Mohr *et al.* (1972).

Magnetite

Magnetite was identified only by XRD, the more clearly so after magnetic concentration of microdrill sub-samples from adjacent to the concretion cores. This is a very minor authigenic reaction product in the concretions, and has not been satisfactorily identified in thin section. As mentioned above, it is one of the predicted corrosion products of metallic iron.

Akaganeite

Akaganeite is the most abundant authigenic cement in the oxidized concretions, but is also present in many of the fresh concretions where it occurs towards their outer parts as a cement in the host sands. In oxidized concretions akaganeite is present throughout the concretion and even occurs in the metallic cores. It is readily identified by XRD, and is shown to be formed from the breakdown of FHC during exposure to air of concretions in the laboratory (see Fig. 5). In thin section akaganeite appears as elongate, bladed opaque crystals that attain lengths of up to 100 μm (Fig. 10a). In the SEM in BSE the bladed morphology of akaganeite is confirmed (Fig. 10b), and akaganeite is seen to post-date all carbonate cements although it is enclosed in gypsum cement. The average of 14 microprobe analyses (listed in Table 1) gave the following structural formula (assuming appropriate hydrogen):

$$Fe_{0.99}O(OH)_{0.84}Cl_{0.16} \quad \text{(compare FeO.OH)}$$

Akaganeite was first reported as a weathering product by M. Nambu (cited by McKay 1962) and named after the

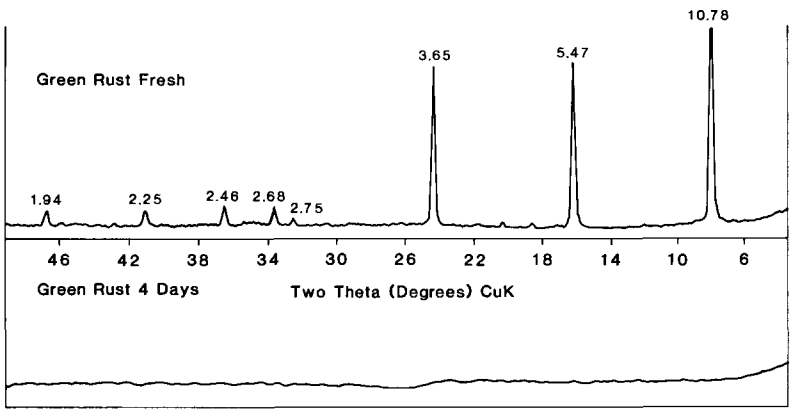

Fig. 9. X-ray diffractograms of corrosion product separated from a concretion core by microdrilling showing the reflections of freshly separated green rust and its total decomposition over a period of 4 days at room temperature in air. Numbers above diagnostic peaks are *d* spacings.

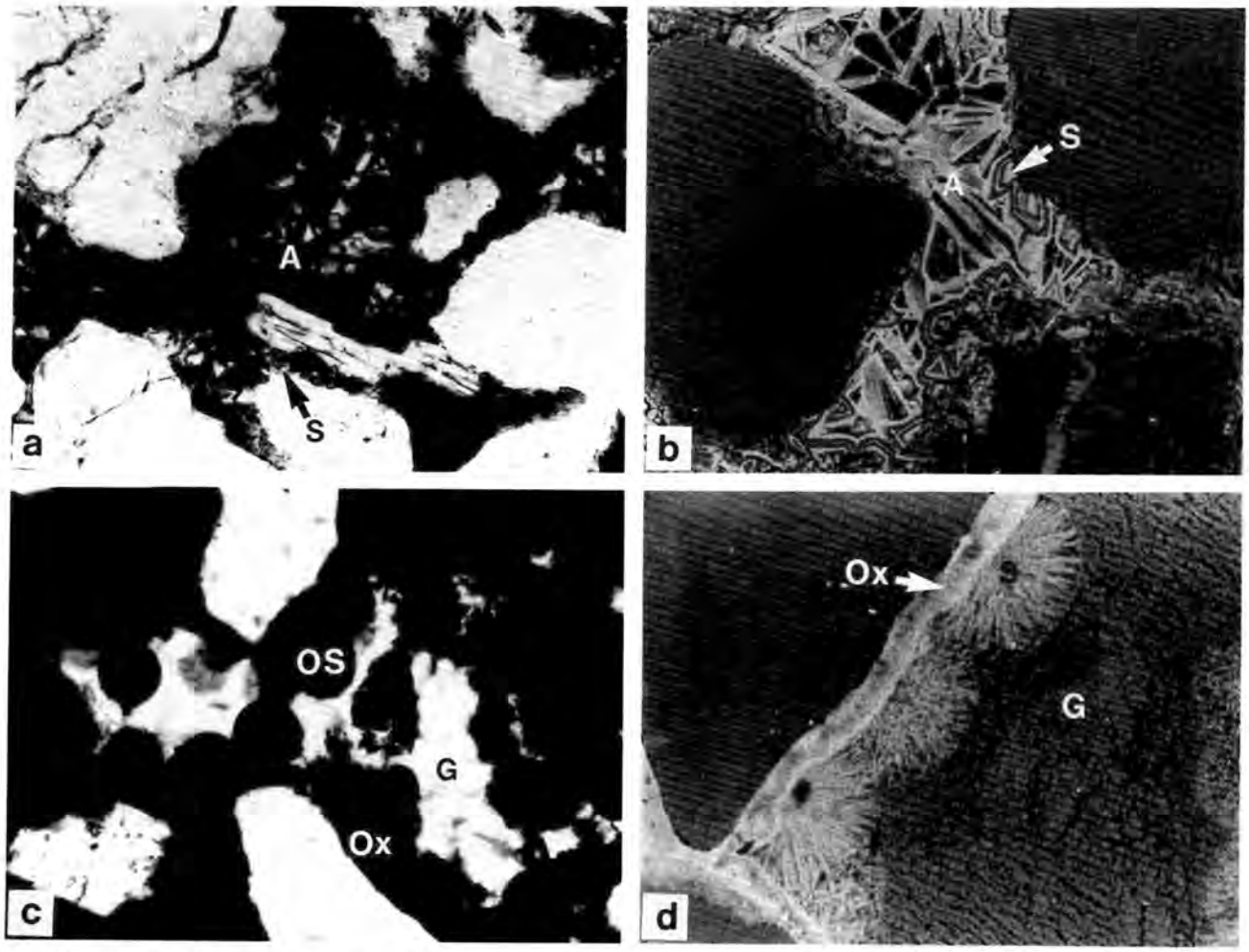

Fig. 10. Optical and BSE-SEM photomicrographs of oxidised cements in the host sand flat sediment. (**a**) Large, opaque bladed crystals of akaganeite (annotated A) enclosing grain rimming rhombic siderite cements (arrowed, S). Transmitted light optical photomicrograph. Width of photomicrograph = 220 μm. (**b**) Corresponding BSE-SEM micrograph showing zoned siderite cement (arrowed, S) enclosed in akaganeite (annotated A). Width of photomicrograph = 180 μm. (**c**) Grain-coating opaque oxidation product (annotated Ox, after monosulphide?), opaque oxidized spheroidal siderite (OS, now probably hematite) together with later pore filling gypsum (annotated G) occupying the centre of pores. Transmitted light optical photomicrograph. Width of photomicrograph = 340 μm. (**d**) Comparable BSE-SEM micrograph of oxidized grain coating material (arrowed Ox), oxidized spheroidal siderite (annotated S) enclosed in poikilotopic gypsum (annotated G). Width of photomicrograph = 180 μm.

Akagane mine in Japan. It has subsequently been noted by several authors (Logan *et al.* 1976; Johnston & Glasby 1978; Rozenson *et al.* 1980; Holm *et al.* 1983; Holm 1984). Pye (1982, 1988) recognized and described akaganeite in concretions at Warham. As mentioned above, significant chlorine is found in akaganeite but its structural location is uncertain.

Based on the laboratory observations of FHC conversion to akaganeite (and the compositional similarity between FHC and akaganeite), alteration of one mineral to the other could be direct (simplified formulae):

$$Fe_5(OH)_9Cl \rightarrow Fe_5O_5(OH)_4Cl + 5H^+ + 5e^- \qquad (13)$$

Texturally, however, FHC and akaganeite are quite dissimilar in their appearance and occurrence in the natural concretions. It is not therefore clear whether the conversion of FHC to akaganeite proceeds via an *in situ* recrystallization process or a dissolution–reprecipitation process. Oxidation would be expected away from the extreme reducing conditions adjacent to the metallic nuclei. The sequence Fe metal → FHC → akaganeite is one of increasing Fe oxidation state: Fe(0) > Fe(II) > Fe(III). The precipitation of akaganeite in the concretions within the Wash sediments thus reflects interaction of the anaerobic metal corrosion environment with the more oxidizing conditions prevailing in the host sediments.

Goethite

Although not detected by XRD, microprobe and SEM-EDS analyses corresponding very closely to FeO.OH were regularly obtained from oxidized concretion zones (average formulae for 11 analyses $Fe_{0.99}O.OH$). They are chemically quite distinguishable from FHC and akaganeite by the absence of chlorine in the analysis.

If this material is goethite, then it is absent from fresh

concretions but is very abundant in concretions that have been naturally oxidized through erosion or artificially oxidized in the laboratory. In thin section goethite is dark red coloured to opaque and is similar in appearance to FHC, and is spatially associated with the nucleus of the concretions. BSE-SEM examination of polished thin sections with the back scatter contrast amplifier set to maximium gain enables a subtle difference between FHC and goethite to be resolved which shows that these two minerals are intimately intergrown in oxidized concretions (see Fig. 4a & b).

Hematite

Hematite is the most stable iron mineral at the Earth's surface and so is expected to form wherever oxygen is readily available. It was identified by XRD in 5 of the 35 concretions studied here, specifically in those recorded during collection of the samples in field as being exposed by erosion. In polished thin section, hematite usually occurs as uniform, equidimensional hexagonal crystals although spheroidal forms are also observed, possibly having formed from oxidation of siderite (Fig. 10c).

Gypsum

Gypsum is overall a quantitatively quite minor component but it is commonly observed around the periphery of the concretions in most of the samples and its presence is confirmed by XRD and chemical analysis. It forms large (millimetre-sized), colourless, poikilotopic crystals that enclose several detrital sand grains. Texturally, gypsum is the youngest authigenic mineral that can be petrographically documented to have formed in the concretions and is observed to enclose all carbonates, akaganeite, goethite and hematite cements (Fig. 10d).

Free access of molecular oxygen to most of the sulphide and carbonate minerals so far described would result in total oxidation of iron to Fe(III) and sulphide to SO_4^{2-}. This reaction is classically seen in the oxidation of pyrite, resulting in dramatic acidification:

$$4FeS_2 + 15O_2 + 8H_2O \rightarrow 2Fe_2O_3 + 16H^+ + 8SO_4^{2-} \quad (14)$$

Gypsum is then precipitated if calcareous shell material or diagenetic calcite is available:

$$CaCO_3 + H_2O + 2H^+ + SO_4^{2-} \rightarrow CaSO_4.2H_2O + CO_2 \quad (15)$$

Gypsum, goethite and hematite represent an extremely common assemblage wherever iron sulphides are exposed to air. This happens most notably, of course, in metalliferous mining spoil tips (Vear & Curtis 1981).

Discussion

Growth of the concretions

The majority of the substantial number of concretions collected in this study contain metallic nuclei. These are fragments of iron and steel left in the sediment by military training exercises that date from the end of the last century. At this time the high tide level along the Lincolnshire coast was almost a kilometre further inland, and sketches of the Freiston Shore Sand Fair of 1844 show a broad expanse of sand flats extending out over what is now saltmarsh and intertidal flats (Robinson 1987). It is this sand surface that was used for military exercises from 1891 and upon which relics of munitions accumulated. Many, perhaps most, became buried by anoxic, muddy sediments as the saltmarsh and higher mudflats prograded across the tidal sands as a result of successive reclamation schemes over the period 1935–1982, and were bathed in anoxic saline pore waters. Anaerobic corrosion at the metal/pore water interface resulted in the precipitation of a ferrous hydroxide-chloride (FHC) and iron monosulphide (FeS) under extremely reducing conditions in which Fe metal at valence state zero was present.

As the FHC corrosion coating developed, its outer surface reacted with the anoxic pore water solutes, HS^- generating more monosulphide, and HCO_3^-, Ca^{2+} and Mg^{2+}, resulting in the precipitation of siderite ($FeCO_3$), ankerite ($Ca(Fe.Mg)(CO_3)_2$) and ferroan calcite ($CaCO_3$).

Around the growing concretions, therefore, a redox gradient was established and was maintained so long as some metal remained in the concretion core. Along this redox gradient the gradual development of very slightly more oxidising conditions variously stabilized elemental sulphur, greigite (Fe_3S_4) and/or pyrite (FeS_2). Green rust ($Fe_3O_4.nH_2O$) and magnetite (Fe_3O_4) were stabilized relative to FHC. The presence of these minerals is further evidence for the action of anaerobic corrosion processes in the concretions.

With time, each corrosion zone expanded and the concretion grew in size. FHC and FeS effectively replaced the metal nucleus inwards by corrosion processes (in this case no sediment was involved) whilst the carbonate cement zone expanded outwards (in this case cementing and incorporating detrital sediment into the concretion). Such reactions would have persisted until all the metal was replaced. Thereafter, the FHC and monosulphides in the central core would presumably be ultimately replaced by green rust and/or magnetite. The former presence of a metallic nucleus in concretions where such reactions progressed to completion can be recognized as the green rust or its oxidation products now pseudomorph the former metal.

Exposure to oxygen when concretions were exhumed (either by marine erosion or by geochemists) resulted in the systematic (from periphery to core) replacement of all the iron minerals by akaganeite, goethite (FeO.OH) or hematite (Fe_2O_3). Sulphides were oxidized in part to sulphuric acid which then reacted with either detrital constituents in the host sediment or authigenic components to precipitate amorphous Fe–Al–Ca basic sulphates (which have not yet been characterized) and gypsum ($CaSO_4.2H_2O$).

Total oxidation of the metallic nucleus would leave an akaganeite–goethite–hematite core to the concretion. The only evidence of the former presence of the metallic nucleus being the absence of incorporated detrital sediment within the hydroxide–oxide core, and the presence of 'ghost' textures preserved during the replacement process.

As the age of the surface on which the concretions are found is well constrained to the nineteenth centuary, and the presence of metallic nuclei supports a rather younger age, the rate of concretion growth can be defined. Concretions of 20 cm diameter are common indicating a growth rate of

around 100 μm per year. This is considerably faster than is calculated for ancient carbonate concretions (Berner 1968; Wilkinson & Dampier 1990).

Wash concretions as analogues for ancient concretions?

The driving force for the growth of siderite–sulphide concretions in the Recent intertidal sediments of the Wash is the presence of metallic iron at valence state zero within anaerobic, saline pore waters of marine origin. This is nothing more than cathodic corrosion that has been well documented for metallic iron artifacts from many marine archaeological sites worldwide (Robinson 1982). Wherever metallic iron is brought into contact with saline, anaerobic waters, cathodic corrosion must take place. In this reaction, anaerobic corrosion generates unstable Fe(II) hydroxides and sulphides which react further with the detrital sediment constituents and marine pore water solutes to precipitate the common-place diagenetic cements (i.e. siderite, ankerite and calcite) as 'secondary' corrosion products. Similar concretions from equivalent intertidal sediments of the north Norfolk coast described by Pye *et al.* (1990) may thus have a comparable origin.

It is the presence of the 'secondary' corrosion products which make the concretions from the Wash similar in terms of their mineralogy and fabric to some ancient concretions. However, the siderite–sulphide concretions in Recent intertidal sediments of the Lincolnshire Wash are the result of anthropogenic contamination and are rather poor analogues for ancient concretions in terms of reaction mechanisms. They have formed by cathodic corrosion of metallic iron and their rapid rate of growth results from the high instability of metallic iron in an anoxic, saline solution and the efficiency of the electrochemical reaction mechanism.

Conclusions

The Wash concretions examined here all appear to have nucleated around metal fragments. The overall mechanisms of authigenic mineral precipitation in these concretions and the driving force for concretion development have been elucidated, although the likely involvement of microbial communities has not been considered and remains a subject for future research. However, the main driving force for concretion growth is the presence of metallic iron at valence state zero within anaerobic, saline pore waters of marine origin. This is the process of cathodic corrosion well documented for many metallic artifacts from marine archaeological sites. Spontaneous anaerobic corrosion generates unstable Fe(II) hydroxides and sulphides which react further with sediment constituents and pore water solutes to precipitate common-place diagenetic cements such as siderite, ankerite and calcite. It is these 'secondary' corrosion products which make these concretions similar in terms of their mineralogy and fabric to some ancient concretions. Their petrographic fabrics, mineralogy, geochemistry and spatial relationships within the concretion, however, are more indicative of the long-term effects of anaerobic, cathodic metal corrosion rather than ancient siderite–sulphide concretion formation. We conclude that siderite–sulphide concretions have formed in Recent intertidal sediments of the Lincolnshire Wash as a result of anthropogenic contamination.

A. and M. Boult at the Freiston Field Centre, Lincolnshire, are thanked for their welcoming hospitality during field seasons. Alan's help and guidance in the field made our understanding of the intertidal flats easier and much more comprehensive than otherwise would have been. His careful reading of an early draft of the manuscript corrected some of our historical misunderstandings of anthropogenic activities around the Wash. J. E. Andrews and T. R. Astin provided constructive reviews.

The University of Manchester is gratefully acknowledged for a University Research Scholarship to MRA-A, who has also been supported by the Palestinian Students Fund, Arab Students' Aid International and the British–Arab Charitable Foundation. British Gas Exploration & Production, Reading (SDB) and the Petroleum Science and Technology Institute, Edinburgh (CDC/SDB) are also thanked for supporting research into geochemical corrosion mechanisms.

References

ADAMS, A. E. & SCHOFIELD, K. 1983. Recent submarine aragonite, magnesian calcite and hematite cements in a gravel from Islay, Scotland. *Journal of Sedimentary Petrology*, **53,** 417–421.

AL-HASHEMI, W. S. 1977. Recent carbonate cementation from sea water in some weathered dolostones, Northumberland, England. *Journal of Sedimentary Petrology*, **47,** 1375–1391.

BERNAL, J. D.; DASGUPTA, D. R. & MACKAY, A. L. 1959. The oxides and hydroxides of iron and their structural interrelationships. *Clay Minerals Bulletin*, **4,** 15–30.

BERNER, R. A. 1968. Rate of concretion growth. *Geochimica et Cosmochimica Acta*, **32,** 477–483

—— 1970. Sedimentary pyrite formation. *American Journal of Science*, **268,** 1–23.

—— 1984. Sedimentary pyrite formation: an update. *Geochimica et Cosmochimica Acta*, **48,** 605–615.

COLEMAN, J. M. & GAGLAINO, S. M. 1965. Sedimentary structures: Mississibi River deltiac plan. *In*: MIDDLETON, G. V. (ed.) *Primary sedimentary structures and their hydrodynamic interpretation*. Special Publications of Society of Economic Paleontologists and Mineralogists, **12,** 133–148.

COLES, B. P. L. & FUNNELL B. M. 1981. Holocene palaeoenvironments of Broadland, England. *In*: NIO, S. D.; SHUTTENHELM, R. T. E. & VAN WEERING, TJ. C. E. (eds) *Holocene marine sedimentation in the North sea basin*. International Association of Sedimentologists, Special Publications, **5,** Blackwell Scientific, Oxford, 123–131.

COLLINS, M. B., AMOS, C. L. & EVANS, G. 1981. Observations of some sediment-transport processes over intertidal flats, the Wash, UK. *In*: NIO, S. D.; SHUTTENHELM, R. T. E. & VAN WEERING, TJ. C. E. (eds) *Holocene marine sedimentation in the North sea basin*. International Association of Sedimentologists, Special Publications, **5,** Blackwell Scientific, Oxford, 81–98.

CURTIS, C. D. & SPEARS, D. A. 1968. The formation of sedimentary iron minerals. Parts I and II. *Economic Geology*, **63,** 257–270.

CURTIS, S. 1987. The history of military use of the Wash. *In*: DOODY, P. & BARNETT, B. (eds) *The Wash and its Environment*. Nature Conservancy Council Research and Survey in Nature Conservation Reports, **7,** NCC, Peterborough, 101–103.

DOODY, P. 1987. The impact of reclamation on the natural environment of the Wash. *In*: DOODY, P. & BARNETT, B. (eds) *The Wash and its Environment*. Nature Conservancy Council Research and Survey in Nature Conservation Reports, **7,** NCC, Peterborough, 165–172.

EVANS, G. 1965. Intertidal flat sediments and their environment of deposition in the Wash. *Quarterly Journal of Geological Society of London*, **121,** 209–245.

—— 1975. Intertidal flat deposits of the Wash, western margins of the North Sea. *In*: GINSBURG, R. N. (ed.) *Tidal Deposits*. 13–20. New York, Springer.

—— & COLLINS, M. B. 1975. The transportation and deposition of suspended sediments over the intertidal flats of the Wash. *In*: HAILS, J. & CARR, A. (eds) *Nearshore sediments dynamics and sedimentation, an Interdisciplinary Review*. Wiley, London, 273–304.

GAUTIER, D. L. 1982. Siderite concretions: indicators of early diagenesis in the Gammon shale Cretaceous. *Journal of Sedimentary Petrology*, **52,** 859–871.

GODWIN, H. & CLIFFORD, M. H. 1938. Studies of the post-Glacial history of British vegetation. I. Origin and stratigraphy of Fenland deposits near Woodwalton, Hunts. *Philosophical Transactions*, **229,** 323–406.

HO, C. & COLEMAN, J. M. 1969. Consolidation and cementation of recent sediments in Atchafalaya Basin. *Geological Society of America Bulletin*, **80,** 183–192.

HOLM, N. G. 1984. The structure of β-FeOOH. Cl akaganite and its uptake of amino acids from Red Sea hot brines. *Origin of Life*, **14,** 343–350.

——, DOWLER, M. J., WADSTEN,T. & ARRHENIUS, G. 1983. β-FeOOH. Cl_n akaganeite and $Fe_{1-x}O$ wustite. in hot brine in the Atlantis II Deep Red Sea and the uptake of the amino acids by synthetic β-FeOOH. Cl_n. *Geochimica et Cosmochimica Acta*, **47,** 1465–1470.

JOHNSTON, J. H. & GLASBY, G. P. 1978. The secondary iron oxide hydroxide mineralogy of some deep sea and fossil manganese nodules: a Mossbauer and X-ray study. *Geochemical Journal*, **12,** 153–164.

JORGENSEN, N. O. 1976. Recent high Mg-calcite-aragonite cementation of beach and submarine sediments from Denmark. *Journal of Sedimentary Petrology*, **46,** 940–951.

LOGAN, N. E., JOHNSTON, J. H. & CHILDS, C. W. 1976. Mossbauer spectrographic evidence for the occurrence of akaganeite in New Zealand soils. *Australian Journal of Soil Research*, **14,** 217–224.

LOVE, L. G. 1967. Early diagenetic iron sulphides in Recent sediments of the Wash England. *Sedimentology*, **9,** 327–352.

MCGILL, I. R., MCENANEY, B. & SMITH, D. C. 1976. Crystal structure of green rust formed by corrosion of cast iron. *Nature*, **259,** 200–201.

MCKAY, A. L. 1962. β-ferric oxyhydroxide-akaganeite. *Mineralogical Magazine*, **33,** 270–280.

MOHR, E. C. J., BAREN, F. A. & SCHUYLENBORGH 1972. *Tropical soils*. 3rd edition. The Hague-Paris-London.

MOORE, S. E., FERRELL, R. E. & AHARONE, P. 1992. Diagenetic siderites and other ferroan carbonates in Modern Subsiding Marsh Sediments. *Journal of Sedimentary Petrology*, **62,** 357–366.

MORSE, J. W., CORNWELL, J. C., ARAKAKI, T., LIN, S. & HUERTA-DIAZ, M. 1992. Iron sulphide and carbonate mineral diagenesis in Baffin Bay, Texas. *Journal of Sedimentary Petrology*, **62,** 671–680.

MOWBRAY, DE T. 1983. The genesis of lateral accretion deposits in Recent intertidal mudflat channels, Solway Firth, Scotland. *Sedimentology*, **30,** 425–435.

NEALSON, K. H. 1983. The microbial iron cycle. *In*: KRUMBEIN, W. E. (ed.) *Microbial Geochemistry*. Blackwell Scientific Publications, London, 159–190.

POSTMA, D. 1977. The occurrence and chemical composition of recent Fe-rich mixed carbonates in river bog. *Journal of Sedimentary Petrology*, **47,** 1089–1098.

—— 1982. Pyrite and siderite formation in brackish and freshwater swamp sediments. *American Journal of Science*, **282,** 1151–1183.

PYE, K. 1982. Marshrock formed by iron sulphide and siderite cementation in saltmarsh sediments. *Nature*, **294,** 650–652.

—— 1988. An occurrence of Akaganeite β-FeOOH.Cl in Recent oxidized carbonate concretions, Norfolk, England. *Mineralogical Magazine*, **52,** 125–126.

——, DICKSON, J. A. D., SCHIAVON, N., COLEMAN, M. L. & COX, M. 1990. Formation of siderite-Mg-calcite-iron sulphide concretions in intertidal marsh and sandflat sediments, north Norfolk, England. *Sedimentology*, **37,** 325–343.

ROBINSON, D. 1987. The Wash: Geographical and historical perspectives. *In*: DOODY, P. & BARNETT, B. (eds) *The Wash and its Environment*. Nature Conservancy Council Research and Survey in Nature Conservation Reports, **7,** NCC, Peterborough. 23–33.

ROBINSON, W. S. 1982. The corrosion and preservation of ancient metals from marine sites. *International Journal of Nautical Archaeology and Underwater Exploration*, **11,** 221–231.

ROZENSON, I., ZAK, I. & SPIRO, B. 1980. The distribution and behaviour of iron in sequence of dolomite, clays and oxides. *Chemical Geology*, **31,** 83–96.

SCHOONEN, M. A. A. & BARNES, H. L. 1991. Reactions forming pyrite and marcasite from solution II: via FeS precursors below 100 °C. *Geochimica et Cosmochimica Acta*, **55,** 1505–1514.

SCHWERTMANN, U. & TAYLOR, R. M. 1977. Iron Oxides. *In*: DIXON, J. & WOOD, S. B. (eds) *Minerals in soil environments*. Soil Science Society of America, 145–180.

SCOTCHMAN, I. C. 1991. The geochemistry of concretions from the Kimmeridge Clay Formation of southern and eastern England. *Sedimentology*, **38,** 79–106.

SHENNAN, I. 1982. Interpretation of Flandrian sea level data from the Fenland, England. *Proceedings of Geologists' Association*, **93,** 53–63.

—— 1986*a*. Flandrian sea level changes in the Fenland I: The geographical setting and evidence of sea level changes. *Journal of Quaternary Science*, **1,** 119–154.

—— 1986*b*. Flandrian sea level changes in the Fenland II: Tendancies of sea level movement, altitudinal changes, local and regional factors. *Journal of Quaternary Science*, **1,** 155–179.

—— 1987. Holocene sea level changes in the North Sea. *In*: TOOLEY, M. J. & SHENNAN, I. (eds) *Sea level changes*. Blackwell, Oxford, 119–151.

STOOPS, G. 1983. SEM and light microscopic observations of minerals in bog ores of the Belgian Campine. *Geoderma*, **30,** 179–186.

SUTTILL, R. G., TURNER, B. & VAUGHAN, D. J. 1982. The geochemistry of iron in Recent tidal-flat sediments of the Wash area, England: a mineralogical Mossbauer and magnetic study. *Geochimica et Cosmochimica Acta*, **46,** 205–217.

SWEENY, R. E. & KAPLAN, I. R. 1973. Pyrite framboid formation: Laboratory synthesis and marine sediments. *Economic Geology*, **68,** 618–634.

SWINNERTON, H. H. & KENT, P. E. 1976. *The Geology of Lincolnshire, 2nd Edition*. Revised by Kent, 1976. Special Publication of Lincolnshire Naturalists Union.

TAKENO, S., ZOKA, H. & NIIHARA 1970. Metastable cubic iron sulphides with special reference to mackinawite. *American Mineralogist*, **55,** 1639–1649.

—— & CLARK, A. H. 1967. Observations on tetragonal Fe, Ni, Co_{1+x} S, mackinawite. *Journal of Science*, Hiroshima University, 5, 287–293.

TAYLOR, R. M. & SCHWERTMANN, U. 1974. Maghemite in soils and its origin. Parts I & II *Clay Minerals*, **10,** 289–298, 299–310.

VAN STRAATEN, L. M. J. U. 1957. Recent sandstone in the coasts of the Netherlands and Rhone delta. *Geologie en Mijnbouw*, **19,** 196–213.

VEAR, A. & CURTIS, C. D. 1981. Quantitative evaluation of pyrite weathering. *Journal of Earth Surface Processes*, **6,** 191–198.

WEIDMANN, H. U. 1972. Shell deposits and shell preservation of in Quaternary and Tertiary estuarine sediments in Georgia, USA. *Sedimentary Geology*, **7,** 103–125.

WILKINSON, M. & DAMPIER, M. D. 1990. The rate of growth of sandstone hosted calcite concretions. *Geochimica et Cosmochimica Acta*, **54,** 3391–3399.

Received 9 January 1993; revised typescript accepted 14 January 1994.